Dependency of Ultrasonic Nakagami Images on The Mechanical Properties of Scattering Medium

Po-Hsiang Tsui[1,2,*,†] Yung-Liang Wan[1,3,†] Yu-Ting Chien[1] Chia-Chun Yeh[1]

Chiao-Yin Wang[1]

[1]*Department of Medical Imaging and Radiological Sciences, College of Medicine, Chang Gung University, Taoyuan 320, Taiwan, ROC*
[2]*Healthy Aging Research Center, Chang Gung University, Taoyuan 320, Taiwan, ROC*
[3]*Department of Medical Imaging and Intervention, Chang Gung Memorial Hospital at Linkou, Taoyuan 333, Taiwan, ROC*

Received 12 Jan 2012; Accepted 5 Apr 2012; doi: 10.5405/jmbe.1101

Abstract

Nakagami images based on backscattered statistics have been demonstrated to complement the ultrasonic B-scan technique for evaluating the arrangements and concentrations of scatterers in the scattering medium. This study explores the relationship between Nakagami images and the mechanical properties of the scattering medium. Experiments were performed on phantoms with various stiffnesses and scatterer concentrations. A commercial supersonic shear imaging system was used to measure the shear modulus of each phantom. The ultrasonic backscattered signals from the phantoms were acquired using a single-element ultrasound scanner for Nakagami imaging. The Nakagami images were compared with the supersonic shear images to explore the dependency of the Nakagami parameter on the medium stiffness. The brightness of the shading in the Nakagami image increased with increasing stiffness of the phantom. For the scattering medium with a low scatterer concentration (8 scatterers·mm^{-3}), the average Nakagami parameter increased from 0.35 to 0.46 when the average shear modulus increased from 11.7 to 167.6 kPa. The average Nakagami parameter measured in the medium with a high scatterer concentration (32 scatterers·mm^{-3}) increased from 0.8 to 0.89 when the shear modulus increased from 12.3 to 174.5 kPa. This study demonstrates that the features of Nakagami images depend on the stiffness of the scattering medium.

Keywords: Nakagami image, Tissue stiffness, Supersonic shear imaging

1. Introduction

Ultrasound grayscale (B-mode) imaging is an important clinical tool for examining the internal structures of tissues [1]. The B-scan intensity is affected by many factors, such as image processing, system settings, and user operations [2,3]. Consequently, B-scan images provide only a primarily qualitative description of morphology, without quantifying tissue properties. The raw ultrasonic radio-frequency (RF) signals backscattered from tissues may contain valuable information that complements the B-scan images for tissue characterization. The statistical properties of backscattered signals depend on the scatterer properties [4-6]. When the resolution cell of the transducer contains a large number of randomly distributed scatterers, the probability density function (pdf) of the backscattered envelope conforms to the Rayleigh distribution [7,8]. If the resolution cell contains scatterers with randomly varying scattering cross-sections, with a comparatively high degree of variance, the envelope statistics conform to a pre- Rayleigh distribution. When the resolution cell contains periodically located scatterers in addition to randomly distributed scatterers, the envelope follows a post-Rayleigh distribution [9]. Non-Rayleigh statistical models, such as Rician [8], K [10], homodyned K [11], and generalized K [12] models, have been developed to encompass the various backscattering conditions.

The Nakagami distribution, initially proposed to describe the statistics of radar echoes [13], has been applied to the statistical analysis of backscattered signals [14-17]. The Nakagami distribution provides a general model for all the backscattering conditions encountered in medical ultrasound. It was found to be strongly related to the statistics of the backscattered signal, with the corresponding Nakagami parameter varying according to the statistics of the backscattered signal [16]. Research has shown that the Nakagami parameter can be used to distinguish various scatterer properties [9,18-20]. Some Nakagami compound distributions, including the Nakagami-Gamma [21,22], Nakagami-lognormal and

† These authors contributed equally to this work
* Corresponding author: Po-Hsiang Tsui
Tel: +886-3-2118800 ext. 3795; Fax: +886-3- 2118700
E-mail: tsuiph@mail.cgu.edu.tw

Nakagami-inverse Gaussian [23], Nakagami-generalized inverse Gaussian [24], and Nakagami Markov random field [25] models, have been developed to provide better fits to the statistical distributions of backscattered-signal envelopes.

The concept of Nakagami imaging based on the Nakagami parameter map originated from the suggestion of Shankar [26] and some other preliminary studies [27,28]. The suggestion arose in response to the need of physicians and radiologists for imaging tools to visually identify scatterer properties in clinical applications. Based on these pilot studies, the present authors previously proposed a standard criterion for constructing the Nakagami image [29], and confirmed its usefulness for tissue characterization in applications such as cataract detection [30], tissue ablation monitoring [31], flow estimation [32,33], breast tumor classification [34,35], cell concentration measurement [36], vocal fold characterization [37], and liver fibrosis assessment [38]. Previous studies have demonstrated that Nakagami images provide information associated with the scatterer arrangement and concentration by reflecting the pdf of the ultrasonic backscattered signals from tissues. This information complements B-scan imaging to improve the diagnosis obtained by conventional ultrasound imaging.

Numerous studies have confirmed that scatterer properties are the key factors in determining the Nakagami parameter and the corresponding imaging features. However, two of our previous studies indicated that features of Nakagami images may also depend on the mechanical properties of tissues to some degree. In one study [30], we explored the feasibility of using Nakagami parametric images to quantify lens stiffness. The experimental results indicated that Nakagami imaging can be used to distinguish both global and local variations in lens stiffness. At that time, it was concluded that the scatterer concentration of the fiber coemption, which is mainly responsible for the increase in lens stiffness during cataract formation, could be quantified using Nakagami images to analyze the statistical distribution of ultrasonic backscattered echoes. In another study [37], we proposed using the Nakagami parameter for the parametric imaging of the biomechanical properties of vocal folds. It was found that the Nakagami images better reflected the anatomical differences of lamina propria and vocal muscle than did B-mode images. We suggested that Nakagami imaging may be used for visualizing the relative concentration of collagen and elastic fibers, which are key factors in determining the biomechanical properties of vocal folds.

These two previous works revealed that the features of Nakagami images may depend on the stiffness of the scattering medium. However, no direct evidence was presented to confirm this. In addition, the underlying mechanism needs to be determined to explain why the features of Nakagami image vary with medium stiffness. This is still an open question in the ultrasound field.

In order to better understand the effects of physical properties on the Nakagami parameter in tissue characterization, the present study explores the relationship between the features of Nakagami images and the mechanical properties of the scattering medium.

2. Materials and methods

2.1 Phantom preparation

Phantoms were made by adding glass beads (59200U, Supelco, Bellefonte, PA, USA) into agar that had been produced by dissolving agar powder in 70 ml of water. The glass beads were used as acoustic scatterers that would produce echoes. The specifications provided by the manufacturers stated that the average diameter of the glass beads was 75 μm. For constructing the phantoms, the agar solution was boiled before the addition of the glass beads. During the cooling period, a stirrer was used to suspend the glass beads in the agar solution to avoid sedimentation. The stirrer was taken out using a magnetic stick before the agar solution solidified. This step ensured that the scatterers were distributed in the phantom as randomly as possible. In order to simulate ultrasound images without and with fully developed speckle patterns, phantoms with scatterer concentrations of 8 and 32 scatterers·mm^{-3} were constructed, respectively. The concentration of scatterers (quantified as the number of scatterers per cubic millimeter) in the phantom was determined using.

$$SC = 3M/(4\pi r_g^3 \rho V) \quad (1)$$

where M, r_g, and ρ correspond to the mass, radius, and density of the glass beads, respectively, and V denotes the volume of the agar phantom. For each scatterer concentration, various percentages by weight of agar powders, namely 0.007%, 0.01%, and 0.02%, were used to produce phantoms with various levels of stiffness. Ten phantoms were made for each stiffness.

2.2 Measurement of phantom stiffness

Prior to the experiments, the mechanical properties of the phantoms with various stiffnesses and scatterer concentrations were estimated using supersonic shear imaging (SSI). The SSI method was described in detail in previous studies [39-41]. Briefly, the SSI method entails generating a remote radiation force by focused ultrasonic beams (i.e., pushing beams). Each pushing beam generates a remote vibration that results in the propagation of a transient shear wave. Several pushing beams at increasing depths are transmitted to generate a quasi-plane shear wave front that propagates throughout the whole imaging area. After the generation of the shear wave, an ultrafast echographic imaging sequence is performed to acquire successive raw data at a very high frame rate to estimate the shear wave velocity and the shear modulus. The stiffer the phantom, the higher the shear modulus is. This study used a commercial shear imaging scanner (Aixplorer, Supersonic, France) with a linear transducer (Model SL15-4, Supersonic, France) that has a bandwidth of 4 to 15 MHz to measure the shear moduli of the phantoms.

2.3 Data acquisition for Nakagami imaging

A single-element ultrasound imaging system, shown in Fig. 1, was constructed to conduct the scanning. It comprised a

mechanical scan assembly, a single-element ultrasound transducer, a pulser/receiver, and a data acquisition card. Mechanical scanning of the ultrasound transducer was implemented using a high-resolution motion stage driven by piezoelectric motors (Model HR8, Nanomotion, Israel). The transducer was driven by a pulser/receiver (Model 5072PR, Panametrics-NDT, Waltham, MA, USA). The received echoes were amplified and filtered with a built-in amplifier and filter in the pulser/receiver. The echoes were then digitized at a sampling rate of 50 MHz by an analog-to-digital converter (Model PXI-5152, National Instruments, Austin, TX, USA) for data storage on a personal computer. The phantom was scanned using a focused transducer with an element diameter of 6 mm (Model V310, Panametrics-NDT). A pulse-echo test of the transducer was carried out. Results showed that the central frequency and the pulse length were 6.5 MHz and 0.3 mm, respectively. The focal length was designed to be 1.1 cm; therefore, the theoretical -6 dB beam width calculated using the f-number was approximately 0.4 mm, as shown in Table 1.

For each phantom, a total of 500 A-lines of backscattered signals were acquired to construct an image. The interval between each scan line was 20 μm, and each scan line was 3 mm. The envelope signal of each scan line was obtained by the Hilbert transform for Nakagami imaging. The algorithm for constructing the ultrasonic Nakagami images was based on our previous study [29]. The Nakagami images of the phantoms were then compared with the results obtained from the supersonic shear images. To explore the relationship between the Nakagami images and the mechanical properties of the scattering medium, a region of interest (ROI) with a size of 1×1 mm^2 was used to acquire local data from the focal zones of images for calculating the average pixel values. The ROIs in both the Nakagami image and the shear wave image were located in the same region in the phantom.

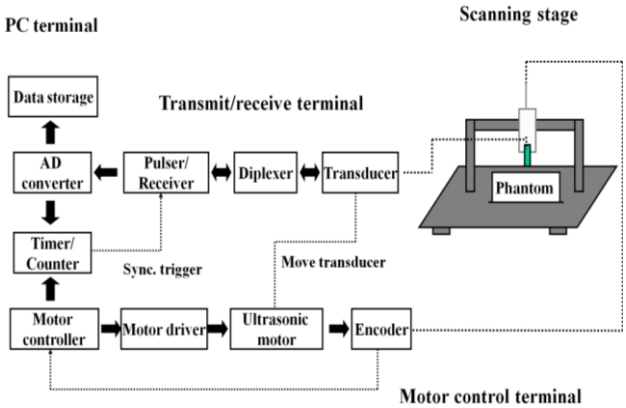

Figure 1. Experimental setup used to acquire raw image data for Nakagami imaging.

Table 1. Characteristics of transducer used in experiments.

Model	V310, Panametrics-NDT, Waltham, MA, USA
Central frequency	6.5 MHz
Focal length	1.1 cm
Element diameter	6 mm
Pulse length	0.3 mm
Beam width	0.4 mm

3. Results

Figure 2 shows the supersonic shear images of the phantoms with various scatterer concentrations and stiffnesses acquired from the shear imaging scanner. The shear wave image display was ranged in a square area with a size of 1 × 1 cm^2. For each scatterer and agar concentration, ten independent phantoms were made; the means and standard deviations of the shear modulus for phantoms with various stiffnesses and scatterer concentrations are summarized in Table 2. The results show that the stiffnesses of the phantoms made from agar powder with a concentration of 0.5 g were 11.7 kPa and 12.3 kPa for scatterer concentrations of 8 and 32 scatterers·mm^{-3}, respectively. When the agar concentrations were 1 g and 1.5 g, the stiffnesses of the phantoms with scatterer concentrations of 8 and 32 scatterers·mm^{-3} were

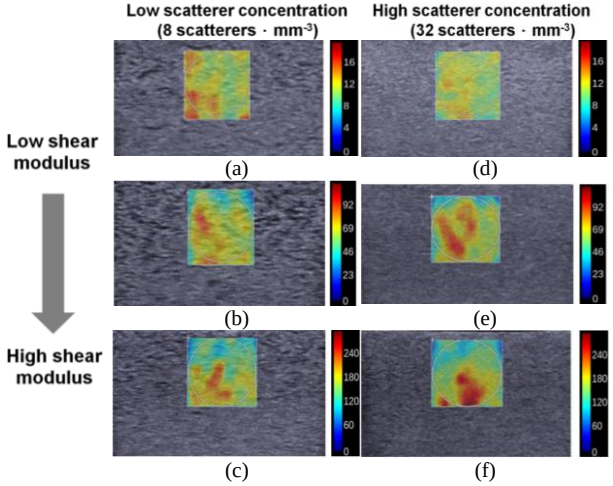

Figure 2. Supersonic shear images of phantoms with different scatterer concentrations and hardnesses. (a)-(c) phantoms with agar concentrations of 0.5 g, 1 g, and 1.5 g respectively, with a scatterer concentration of 8 scatterers·mm^{-3}. (d)-(f) phantoms with agar concentrations of 0.5 g, 1 g, and 1.5 g respectively, with a scatterer concentration of 32 scatterers·mm^{-3}.

Table 2. Shear moduli of phantoms with various scatterer and agar concentrations measured by supersonic shear imaging. Data are expressed as mean ± standard deviation calculated from ten independent phantoms.

Scatterer concentration \ Agar concentration	0.5 g	1.0 g	1.5 g
8·mm^{-3}	11.7 ± 0.3 kPa	69.8 ± 1.4 kPa	167.6 ± 4.1 kPa
32·mm^{-3}	12.3 ± 0.7 kPa	74.3 ± 2.6 kPa	174.5 ± 2.7 kPa

roughly 70 kPa and 170 kPa, respectively. The results indicate that the scatterer concentration did not significantly affect the phantom stiffness for a given concentration of agar powder. The phantom stiffness increased with the concentration of agar powder.

Phantoms with stiffnesses ranging from approximately 12 kPa to 170 kPa were thus constructed, as validated by the supersonic shear imaging. The next step was to study the dependence of the Nakagami image features on the medium

stiffness. Figure 3 shows typical Nakagami images and Nakagami parameter values for phantoms with various stiffnesses. In this example, the phantoms had scatterer concentrations of 8 scatterers·mm^{-3}. Prior research has shown that a scattering medium with a low scatterer concentration displays relatively few scatterers in the resolution cell of the focused transducer [29]. This finding explains why phantoms with different stiffnesses had different levels of blue shading in their Nakagami images, indicating that globally backscattered statistics form a pre-Rayleigh distribution (average $m_w < 1$). In principle, a given scatterer concentration results in similar features and shadings in the Nakagami image. However, it was observed that the brightness of the blue shading in the Nakagami image gradually increased as the stiffness of the phantom increased. To verify this, the values of all pixels in the Nakagami image were used to calculate the average Nakagami parameter. The average Nakagami parameter increased from 0.35 to 0.46 when the average shear modulus increased from 11.7 kPa to 167.6 kPa. The probability value (i.e., *p*-value) obtained from Student's *t*-test indicates that the Nakagami parameter corresponding to each shear modulus was significantly different ($p < 0.05$). Based on the experimental observations, a linear fitting was used to describe the relationship between the Nakagami parameter and the shear modulus. The correlation coefficient obtained from the linear fitting was 0.83, demonstrating that the Nakagami parameter measured in a medium with a low scatterer concentration correlated strongly with the stiffness of the medium.

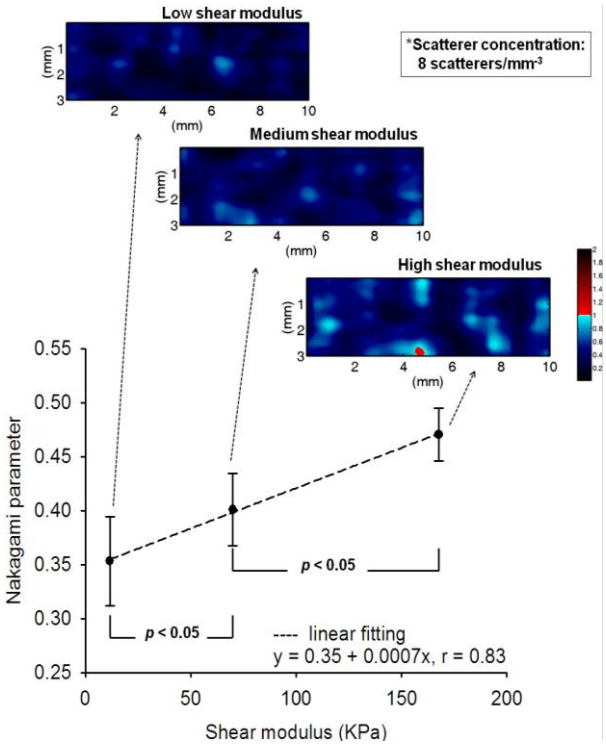

Figure 3. The Nakagami images and the Nakagami parameters under different medium hardnesses (scatterer concentration of 8 scatterers·mm^{-3}).

The dependence of the features of Nakagami images measured in a medium with a high scatterer concentration on the medium stiffness was also investigated. For a scatterer concentration of 32 scatterers·mm^{-3}, typical Nakagami images and Nakagami parameter values for phantoms with varying stiffnesses are shown in Fig. 4. Previous research found that a high concentration of scatterers may easily result in a large number of scatterers within the resolution cell of even a highly focused ultrasound transducer, which means that the global backscattered-signal statistics tend to approach a Rayleigh distribution, corresponding to red and blue shading (average $m_w \approx 1$) [29,31]. Here, the shading in the Nakagami images changed slightly with increasing phantom stiffness. Quantitative analysis of the Nakagami images revealed that the average Nakagami parameter increased from 0.8 to 0.89 when the shear modulus increased from 12.3 kPa to 174.5 kPa. To compare these results with those in Fig. 3, a linear equation was used to fit the curve of the Nakagami parameter as a function of shear modulus. The correlation coefficient was 0.53, implying that the Nakagami parameter measured in a medium with a high scatterer concentration did not highly depend on medium stiffness. The *p*-value analysis also showed that the average Nakagami parameter values of mediums with shear moduli smaller than 74.3 KPa were statistically indistinguishable ($p > 0.05$).

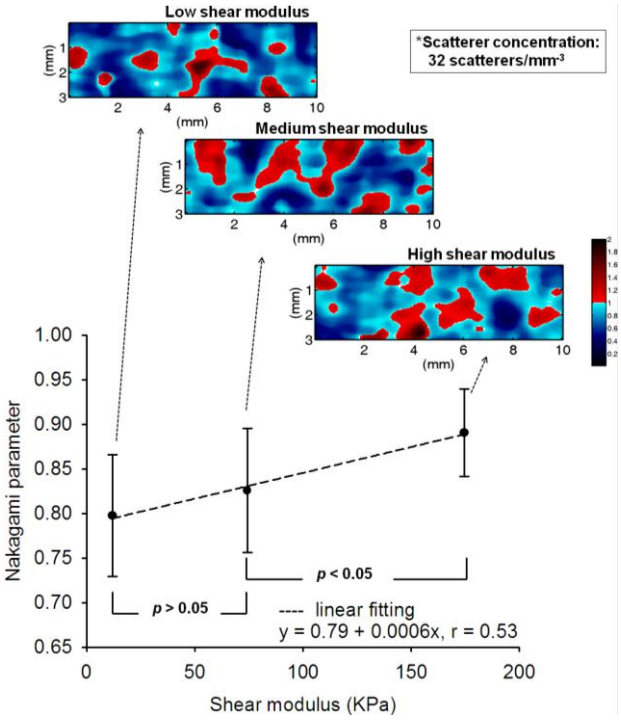

Figure 4. The Nakagami images and the Nakagami parameters under different medium hardnesses (scatterer concentration of 32 scatterers·mm^{-3}).

4. Discussion

The present study is the first to document the effect of medium stiffness on the Nakagami image and parameter estimated from ultrasonic backscattered signals. This study clarified the relationship between the Nakagami parametric image and the mechanical properties of the scattering medium. The estimation of the Nakagami parameter depends on the

medium stiffness, as evidenced by phantom experiments.

According to the experimental results, the Nakagami parameter appears to increase with increasing stiffness of the medium; therefore, the shadings and features in the Nakagami image vary with the medium stiffness. Explaining why the medium stiffness influences the Nakagami parameter is necessary for understanding the physical meanings of Nakagami images in ultrasonic tissue characterization. Research has shown that the estimations of the ultrasound statistical parameters are determined by the number of scatterers in the resolution cell of the transducer [19,42,43]. The size of the resolution cell is defined by the beam cross-sectional area and the transducer pulse length [43]. The degree of transducer focusing directly influences the size of the resolution cell, which in turn affects the first-order statistical properties of ultrasonic echoes relative to the effective number of scatterers in the resolution cell [19,42-44]. In other words, the Nakagami parameter depends on the medium stiffness possibly due to variations in the medium stiffness affecting the size of the transducer resolution cell.

The velocity of sound is known to depend on both the stiffness and the density of the medium. Greater medium stiffness corresponds to a higher sound velocity. In each phantom measurement, the same experimental settings were used to acquire the backscattered signals from the focal zone of the transducer. This meant that the effect of acoustic attenuation due to beam diffraction could be ignored; therefore, the downshift of the ultrasound frequency caused by the attenuation effect [45] did not occur. To verify this, the Fourier transform was applied to obtain the frequency spectra of the backscattered signals returned from the phantoms with various scatterer concentrations and stiffnesses. The results, shown in Fig. 5, indicate that the center frequencies of echo signals from different phantoms were almost the same, indicating that no frequency downshift occurred. When the sound velocity increases but the frequency does not change, the wavelength increases accordingly. The increase in wavelength implies an increase in the transducer pulse length, which can be calculated by multiplying the wavelength by the number of cycles in one transmitting pulse. In this condition, the transducer tends to have a larger resolution cell to contain more scatterers, resulting in an increase in the Nakagami parameter.

Although the Nakagami parameter increases with increasing the shear modulus, the effect of the medium stiffness on the estimation of the Nakagami parameter seems to be weak when the scattering medium has a high scatterer concentration. This is supported by a comparison between Figs. 4 and 5, which indicates that the correlation coefficient between the Nakagami parameter and the shear modulus of the medium largely decreased from 0.83 to 0.53 when the scatterer concentration changed from low to high. This may be due to the increment in the number of scatterers in the resolution cell caused by increased medium stiffness having different degrees of impact on the Nakagami parameter with different scatterer concentrations. When the medium has a high scatterer concentration, the resolution cell already contains a lot of scatterers (this is why the Nakagami parameter was close to 1 in Fig. 4). Thus, the effect of the increment in the number of scatterers in the resolution cell on estimating the Nakagami parameter may be limited. In contrast, the resolution cell has a small number of scatterers for a medium with a low scatterer concentration. The change in the Nakagami parameter may be more sensitive to an increase in the number of scatterers due to the expansion of the resolution cell.

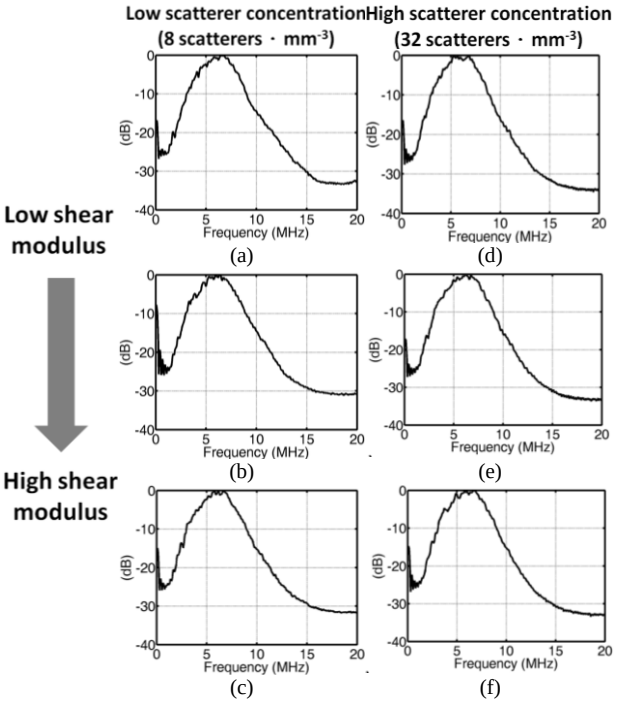

Figure 5. Fourier spectrums of the ultrasonic backscattered signals from phantoms with different scatterer concentrations and hardnesses. (a)-(c) spectrums of the phantoms with agar concentrations of 0.5 g, 1 g, and 1.5 g respectively, with a scatterer concentration of 8 scatterers·mm^{-3}. (d)-(f) spectrums of the phantoms with agar concentrations of 0.5 g, 1 g, and 1.5 g with a scatterer concentration of 32 scatterers·mm^{-3}.

It is interesting to discuss which factor (scatterer concentration or stiffness) dominates the estimation of the Nakagami parameter. In Fig. 3, the slope of the fitting curve indicates that the Nakagami parameter increases only 0.0007 when the shear modulus increases 1 kPa. Such a low sensitivity of the Nakagami parameter to the variation of the medium stiffness can also be found in Fig. 4. The results of the linear fitting imply that only a strong increase in the stiffness of the medium can produce a significant change in the Nakagami parameter and thus influence the shading of the Nakagami image. Tissues with different pathologies have different ranges of shear modulus. For instance, the range of the shear modulus for human liver tissues, including fibrosis cases, is approximately between 5 and 50 kPa [41]. Normal breast tissue has a shear modulus of below 10 kPa, whereas malignant tumors have quite a high shear modulus of between 150 and 175 kPa [39]. In other words, the Nakagami parameter and Nakagami images do not necessarily reflect the variations of the stiffness for different tissues. The average Nakagami parameter values for benign and malignant breast tumors are 0.7 and 0.58, respectively [35]. According to the above

discussion and the comparison of references [35] and [39], it can be stated that the scatterer concentration (or arrangement) dominates the Nakagami parameter estimation and the Nakagami image formation.

5. Conclusion

This study explored the relationship between Nakagami images and the mechanical properties of the scattering medium. Nakagami images were compared with supersonic shear images of phantoms with various scatterer concentrations and stiffnesses. For a given scatterer concentration, the Nakagami parameter increased with increasing shear modulus of the medium, making the shading of the Nakagami image brighter. The Nakagami parameter varies with the medium stiffness possible due to the change in the size of the transducer resolution cell caused by the change in the sound speed. This paper demonstrated that the features of Nakagami images depend on the medium stiffness. The above findings may be helpful to physicians and researchers for explaining clinical results and the mechanism of tissue characterization using Nakagami images.

Acknoledgements

This work was supported by the National Science Council of the Republic of China (Taiwan) under grants NSC 100-2628-E-182-003-MY2 and NSC 100-3114-B-002-004.

References

[1] K. K. Shung, "Diagnostic ultrasound: past, present, and future," *J. Med. Biol. Eng.*, 31: 371-374, 2011.
[2] D. A. Christensen, *Ultrasonic Bioinstrumentation*, New York: Wiley, 1988.
[3] T. L. Szabo, *Diagnostic ultrasound imaging*, Burlington, MA: Elsevier Academic Press, 2004.
[4] J. C. Bamber and C. R. Hill, "Acoustic properties of normal and cancerous human liver-I dependence on pathological condition," *Ultrasound Med. Biol.*, 7: 121-133, 1981.
[5] J. C. Bamber, C. R. Hill and J. A. King, "Acoustic properties of normal and cancerous human liver-II dependence on tissue structure," *Ultrasound Med. Biol.*, 7: 135-144, 1981.
[6] M. F. Insana, R. F. Wagner, D. G. Brown and T. J. Hall, "Describing small-scale structure in random media using pulse-echo ultrasound," *J. Acoust. Soc. Am.*, 87: 179-192, 1990.
[7] C. B. Burckhardt, "Speckle in ultrasound B-mode scans," *IEEE Trans. Sonics Ultrason.*, 25: 1-6, 1978.
[8] R. F. Wagner, M. F. Insana and D. G. Brown, "Statistical properties of radio-frequency and envelope detected signals with applications to medical ultrasound," *J. Opt. Soc. Am. A-Opt. Image Sci. Vis.*, 4: 910-922, 1987.
[9] P. M. Shankar, V. A. Dumane, J. M. Reid, V. Genis, F. Forsberg, C. W. Piccoli and B. B. Goldberg, "Classification of ultrasonic B-mode images of breast masses using Nakagami distribution," *IEEE Trans. Ultrason. Ferroelectr. Freq. Control*, 48: 569-580, 2001.
[10] L. Weng, J. M. Reid, P. M. Shankar and K. Soetanto, "Ultrasound speckle analysis based on the K distribution," *J. Acoust. Soc. Am.*, 89: 2992-2995, 1991.
[11] V. Dutt and J. F. Greenleaf, "Ultrasound echo envelope analysis using a homodyned K distribution signal model," *Ultrason. Imaging*, 16: 265-287, 1994.
[12] P. M. Shankar, "A model for ultrasonic scattering from tissues based on K-distribution," *Phys. Med. Biol.*, 40: 1633-1649, 1995.
[13] H. C. Holfman, *Statistical methods on radio wave propagation*, New York: Pergamon Press, 1960.
[14] C. C. Huang, "Detecting spatial variations of erythrocytes by ultrasound backscattering statistical parameters under pulsatile flow," *IEEE Trans. Biomed. Eng.*, 58: 1163-1171, 2011.
[15] C. C. Huang, Y. H. Lin and S. H. Wang, "The effect of kinetic properties on statistical variations of ultrasound signals backscattered from flowing blood," *Jpn. J. Appl. Phys.*, 48: 027002-1-027002-7, 2009.
[16] P. M. Shankar, "A general statistical model for ultrasonic backscattering from tissues," *IEEE Trans. Ultrason. Ferroelectr. Freq. Control*, 47: 727-736, 2000.
[17] M. P. Wachowiak, R. Smolikova, G. D. Tourassi and A. S. Elmaghraby, "General ultrasound speckle models in determining scatterer density," *Proc. Sci. Comp. Sci. Appli. Engi.*, 4687: 285-295, 2002.
[18] P. M. Shankar, V. A. Dumane, C. W. Piccoli, J. M. Reid, F. Forsberg and B. B. Goldberg, "Computer-aided classification of breast masses in ultrasonic B-scans using a multiparameter approach," *IEEE Trans. Ultrason. Ferroelectr. Freq. Control*, 50: 1002-1009, 2003.
[19] P. H. Tsui and S. H. Wang, "The effect of transducer characteristics on the estimation of Nakagami parameter as a function of scatterer concentration," *Ultrasound Med. Biol.*, 30: 1345-1353, 2004.
[20] P. H. Tsui, Y. L. Wan, C. C. Huang and M. C. Wang, "Effect of adaptive threshold filtering on ultrasonic Nakagami parameter to detect variation in scatterer concentration," *Ultrason. Imaging*, 32: 229-242, 2010.
[21] P. M. Shankar, "A compounding scattering pdf for the ultrasonic echo envelope and its relationship to K and Nakagami distributions," *IEEE Trans. Ultrason. Ferroelectr. Freq. Control*, 50: 339-343, 2003.
[22] P. M. Shankar, "The use of the compounding probability density function in ultrasonic tissue characterization," *Phys. Med. Biol.*, 49: 1007-1015, 2004.
[23] Karmeshu and R. Agrawal, "Study of ultrasonic echo envelope based on Nakagami-inverse Gaussian distribution," *Ultrasound Med. Biol.*, 32: 371-376, 2006.
[24] R. Agrawal and Karmeshu, "Ultrasonic backscattering in tissue: characterization through Nakagami-generalized inverse Gaussian distribution," *Comput. Biol. Med.*, 37: 166-172, 2006.
[25] N. Bouhlel and S. Sevestre-Ghalila, "Nakagami Markov random field as texture model for ultrasound RF envelope model," *Comput. Biol. Med.*, 39: 535-544, 2009.
[26] P. M. Shankar, "Statistical modeling of scattering from biological media," *J. Acoust. Soc. Am.*, 111: 2463, 2002.
[27] R. Kolar, R. Jirik and J. Jan, "Estimator comparison of the Nakagami-m parameter and its application in echocardiography," *Radioengineering*, 13: 8-12, 2004.
[28] F. Davignon, J. F. Deprez and O. Basset, "A parametric imaging approach for the segmentation of ultrasound data," *Ultrasonics*, 43: 789-801, 2005.
[29] P. H. Tsui and C. C. Chang, "Imaging local scatterer concentrations by the Nakagami statistical model," *Ultrasound Med. Biol.*, 33: 608-619, 2007.
[30] P. H. Tsui, C. C. Huang, C. C. Chang, S. H. Wang and K. K. Shung, "Feasibility study of using high-frequency ultrasonic Nakagami imaging for characterizing the cataract lens in vitro," *Phys. Med. Biol.*, 52: 6413-6425, 2007.
[31] P. H. Tsui, C. K. Yeh, C. C. Chang and W. S. Chen, "Performance evaluation of ultrasonic Nakagami image in tissue characterization," *Ultrason. Imaging*, 30: 78-94, 2008.
[32] P. H. Tsui, C. K. Yeh and C. C. Chang, "Microvascular flow estimation by microbubble-assisted Nakagami imaging," *Ultrasound Med. Biol.*, 35: 653-671, 2009.
[33] P. H. Tsui, C. K. Yeh and C. C. Chang, "Microvascular flow estimation by contrast-assisted B-scan and statistical parametric images," *IEEE Trans. Inf. Technol. Biomed.*, 13: 360-369, 2009.

[34] P. H. Tsui, C. K. Yeh, C. C. Chang and Y. Y. Liao, "Classification of breast masses by ultrasonic Nakagami imaging," *Phys. Med. Biol.*, 53: 6027-6044, 2008.

[35] P. H. Tsui, Y. Y. Liao, C. C. Chang, W. H. Kuo, K. J. Chang and C. K. Yeh, "Classification of benign and malignant breast tumors by 2-D analysis based on contour description and scatterer characterization," *IEEE Trans. Med. Imaging*, 29: 513-522, 2010.

[36] S. H. Chen, Y. H. Lin, W. T. Li, S. H. Wang and C. C. Huang, "Estimation of cell concentration using high-frequency ultrasonic backscattering," *J. Med. Biol. Eng.*, 32: 157-162, 2012.

[37] P. H. Tsui, C. C. Huang, L. Sun, S. H. Dailey and K. K. Shung, "Characterization of lamina propria and vocal muscle in human vocal fold tissue by ultrasound Nakagami imaging," *Med. Phys.*, 38: 2019-2026, 2011.

[38] M. C. Ho, J. J. Lin, Y. C. Shu, C. N. Chen, K. J. Chang, C. C. Chang and P. H. Tsui, "Using ultrasound Nakagami imaging to assess liver fibrosis in rats," *Ultrasonics*, 52: 215-222, 2012.

[39] M. Tanter, J. Bercoff, A. Athanasiou, T. Deffieux, J. L. Gennisson, G. Montaldo, M. Muller, A. Tardivon and M. Fink, "Quantitative assessment of breast lesion viscoelasticity: initial clinical results using supersonic shear imaging," *Ultrasound Med. Biol.*, 34: 1373-1386, 2008.

[40] M. Muller, J. L. Gennisson, T. Deffieux, M. Tanter and M. Fink, "Quantitative viscoelasticity mapping of human liver using supersonic shear imaging: preliminary in vivo feasibility study," *Ultrasound Med. Biol.*, 35: 219-229, 2009.

[41] E. Bavu, J. L. Gennisson, M. Couade, J. Bercoff, V. Mallet, M. Fink, A. Badel, A. Vallet-Pichard, B. Nalpas, M. Tanter and S. Pol, "Noninvasive in vivo liver fibrosis evaluation using supersonic shear imaging: a clinical study on 113 hepatitis C virus patients," *Ultrasound Med. Biol.*, 37: 1361-1373, 2011.

[42] T. A. Tuthill, R. H. Sperry and K. J. Parker, "Deviations from Rayleigh statistics in ultrasonic speckle," *Ultrason. Imaging*, 10: 81-89, 1988.

[43] J. A. Zagzebski, J. F. Chen, F. Dong and T. Wilson, "Intervening attenuation affects first-order statistical properties of ultrasound echo signals," *IEEE Trans. Ultrason. Ferroelec. Freq. Contr.*, 46: 35-40, 1999.

[44] J. F. Chen, J. A. Zagzebski and E. L. Madsen, "Non-Gaussian versus non-Rayleigh statistical properties of ultrasound echo signals," *IEEE Trans. Ultrason. Ferroelectr. Freq. Control*, 41: 435-440, 1994.

[45] P. D. Bevan and M. D. Sherar, "B-scan ultrasound imaging of thermal coagulation in bovine liver: frequency shift attenuation mapping," *Ultrasound Med. Biol.*, 27: 809-817, 2001.